Optical sparse aperture imaging

Nicholas J. Miller,[1,*] Matthew P. Dierking,[2] and Bradley D. Duncan[1]

[1]Electro Optics Program, University of Dayton, 300 College Park, Dayton Ohio 45469-0245, USA
[2]Air Force Research Laboratory, AFRL/SNJM, 3109 Hobson Way, Building 622, Wright-Patterson Air Force Base, Ohio 45433-7700, USA

*Corresponding author: nicholas.miller@wpafb.af.mil

Received 8 March 2007; accepted 13 April 2007;
posted 25 April 2007 (Doc. ID 80775); published 9 August 2007

The resolution of a conventional diffraction-limited imaging system is proportional to its pupil diameter. A primary goal of sparse aperture imaging is to enhance resolution while minimizing the total light collection area; the latter being desirable, in part, because of the cost of large, monolithic apertures. Performance metrics are defined and used to evaluate several sparse aperture arrays constructed from multiple, identical, circular subapertures. Subaperture piston and/or tilt effects on image quality are also considered. We selected arrays with compact nonredundant autocorrelations first described by Golay. We vary both the number of subapertures and their relative spacings to arrive at an optimized array. We report the results of an experiment in which we synthesized an image from multiple subaperture pupil fields by masking a large lens with a Golay array. For this experiment we imaged a slant edge feature of an ISO12233 resolution target in order to measure the modulation transfer function. We note the contrast reduction inherent in images formed through sparse aperture arrays and demonstrate the use of a Wiener–Helstrom filter to restore contrast in our experimental images. Finally, we describe a method to synthesize images from multiple subaperture focal plane intensity images using a phase retrieval algorithm to obtain estimates of subaperture pupil fields. Experimental results from synthesizing an image of a point object from multiple subaperture images are presented, and weaknesses of the phase retrieval method for this application are discussed.

OCIS codes: 110.1220, 110.5100, 110.4100, 100.5070.

1. Introduction

Sparse aperture imaging has grown out of the quest for higher angular resolutions in astronomy. The field of sparse aperture interferometry is a relatively mature technology. Since the 1940s, radio interferometers have been successfully built, which combine radiation fields from multiple antennae. These allow the synthesis of higher resolution images of extraterrestrial radio sources than would be possible from any individual antenna. Antenna arrays such as the very large array (VLA) can be used to synthesize high resolution two-dimensional images of radio sources by measuring their complex visibility [1]. Through inversion of the Fourier amplitude and phase visibility, an image of the source is synthesized [2].

0003-6935/07/235933-11$15.00/0

Applying sparse aperture imaging techniques to optical wavelength imaging systems presents unique challenges. In radio interferometry, the interference and correlation of the radiation fields from each subantenna are normally performed postdetection. The phasing of the signals from each subantenna in the RF array is often accomplished through the relatively simple insertion of appropriate delay lines between the antennas and the correlator. This is not possible with optical arrays because present detector technology is capable of recording only the time averaged intensity of the optical field at each subaperture rather than coherently detecting both field amplitude and phase, as is the case with RF arrays. Therefore, the optical fields themselves are interfered on a single focal plane detector array. This interferometric beam combination necessitates phasing of the subapertures to within a fraction of a wavelength. Relatively short optical wavelengths therefore require high positioning accuracy for the phasing and alignment of each optical subaperture.

Michelson's stellar interferometer is an early example of what is essentially a two element sparse aperture configuration at optical wavelengths. Using two mirrors, Michelson sampled a narrow band of spatial frequencies along one direction [3]. By changing the distance between the two mirrors (the baseline) Michelson recorded the contrast, or fringe visibility, at multiple spatial frequencies. Had he been able to measure the fringe phase at each spatial frequency as well, he could have constructed one-dimensional images of interstellar sources. Instead, he assumed the sources were stars with circularly symmetric brightness profiles. By noting the baseline distance when the fringe visibility was extinguished, he calculated the angular diameters of stars.

The resolution of conventional monolithic apertures is well described by a single measure, the width of the central peak of the point spread function (PSF), which is in turn inversely proportional to the pupil diameter. This measure is often of interest to astronomers desiring improved angular resolution but is inadequate in the analysis of an imaging system where targets of interest are extended objects with significant spatial frequency content and often with less contrast. The modulation transfer function (MTF) developed from Fourier analysis is also used to quantitatively judge the merit of sparse aperture arrays and is particularly useful in light of the possibility of postprocessing deconvolution to obtain an image equivalent in resolution to that of a single filled aperture. A primary goal of sparse aperture imaging is to enhance resolution while minimizing the total light collection area, the latter being desirable because of the cost of large monolithic apertures.

In Section 2, quantitative metrics based on the PSF and MTF are developed to evaluate sparse aperture arrays constructed from multiple, identical, circular subapertures. In Section 3, we select arrays constructed on the compact nonredundant point arrays described by Golay [4]. We vary both the number of subapertures and their relative spacings to arrive at an optimal array. In Section 4, the effects of piston and/or tilt aberrations are investigated as they relate to sparse aperture imaging. In Section 5, we report the results of synthesizing an image from multiple subaperture pupil fields by masking a large lens with a Golay array, noting the contrast reduction inherent to sparse arrays. In Section 6, we examine the postdetection synthesis of multiple focal plane subimages. A synthesis method using a phase retrieval algorithm is described and experimental results for point source imaging are presented. Weaknesses of this phase retrieval method are also discussed. Our conclusions are presented in Section 7.

2. Theory

We choose to examine Golay-N sparse aperture imaging arrays comprised of N identical, circular,

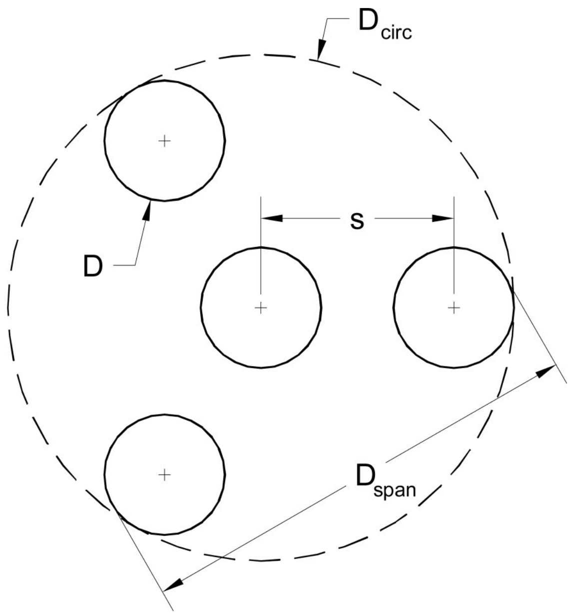

Fig. 1. Golay-4 array with expansion factor of 1.6.

diffraction-limited subaperture pupils. Figure 1 shows an example sparse array consisting of four subapertures. We define s to be the distance between the centers of the most closely spaced subapertures. D is the diameter of each subaperture, and the ratio s/D will be known as the array's expansion factor. The sparse aperture arrays evaluated in this study will consist of unit diameter subapertures so that the expansion factor is simply s. For example, arrays with tangent subapertures possess the smallest allowable expansion factor of unity. Moreover, D_{span} defines the maximum baseline dimension in the pupil array and D_{circ} is the minimum diameter of a circle that circumscribes the entire array.

A good sparse aperture design combines the optical fields from its subapertures to obtain a resolution equivalent to that of a single filled aperture with a large effective area A_{eff}. A good array design maximizes A_{eff} while minimizing the total collection area A_{array}. The fill factor α is the ratio of the area of the sparse aperture array to the area of a single filled aperture whose image resolution best matches the image resolution of the sparse array. Therefore, the merit of a sparse aperture array lies in minimizing the fill factor α. For sparse arrays composed of N identical, unit diameter, circular subapertures the fill factor is given by

$$\alpha = \frac{N}{D_{eff}^2}, \tag{1}$$

where D_{eff} is the effective diameter of a single filled circular aperture that best matches the image quality of the sparse aperture design. However, there is not a clear consensus on how to quantify D_{eff}, as resolution can be judged according to various focal plane metrics, such as the Sparrow or Rayleigh criteria, or by examining spatial frequency metrics [5–10].

A. Focal Plane (Point Spread Function) Metrics

A sparse array pupil function, $P_{array}(x, y)$, consisting of N identical, except possibly for phase, subapertures in the (x, y) plane can be written as,

$$P_{array}(x,\ y) = \sum_{n=1}^{N} P_{sub}(x - x_n,\ y - y_n)e^{j\phi_n(x,y)}, \qquad (2)$$

where $P_{sub}(x, y)$ is the common modulus of all subaperture pupil functions and where $\phi_n(x, y)$ is the phase structure, and (x_n, y_n) are the center coordinates of the nth subaperture, respectively. Imaging can be thought of as an interferometric process where spatial frequencies are sampled based on the vector distance between points in the pupil. An N point pupil array has $N(N - 1)/2$ combinations of pupil point pair vector distances. Through Fourier analysis and application of the autocorrelation theorem then, the incoherent PSF of any sparse aperture array consisting of N identical, diffraction-limited, in-phase, (i.e. all $\phi_n = 0$) subapertures is given by

$$\mathrm{PSF}_{array}(u,\ v) = \mathrm{PSF}_{sub}(u,\ v)\left[N + 2\sum_{k=1}^{N(N-1)/2} \times \cos\left[\frac{2\pi}{\lambda f}(\Delta x_k u + \Delta y_k v)\right]\right], \qquad (3)$$

where (u, v) are the image plane coordinates, $(\Delta x_k, \Delta y_k)$ are the vector separation components between pairs of subaperture centers, λ is the wavelength, and f is the distance from the pupil to the image plane.

An incoherent imaging system is linear in intensity so that the image formed is the convolution of the pupil array PSF and the ideal geometric image intensity. In the ideal geometric limit, the array PSF would be a delta function. Therefore, both a narrow PSF central peak and minimization of energy outside the central peak are desirable. One method for defining D_{eff} can thus be based on the full width at half maximum (FWHM) of the PSF according to

$$D_{eff(PSF)} = \frac{\delta_0}{\mathrm{FWHM}_{array\ PSF}} = \frac{1.03\lambda f}{\mathrm{FWHM}_{array\ PSF}}, \qquad (4)$$

where δ_0 is the FWHM of the PSF of a single unit diameter aperture.

Now note that the $\mathrm{FWHM}_{array\ PSF}$ is approximately inversely proportional to the maximum baseline array dimension, D_{span}. However, if the expansion factor is increased in order to increase D_{span}, the decreased fill factor will also result in less energy in the central peak. The ratio of energy contained in the PSF central peak versus the energy in the sidelobes is also of great interest. We therefore adopt a measure, called the peak-to-integrated-sidelobe-ratio (PISLR),

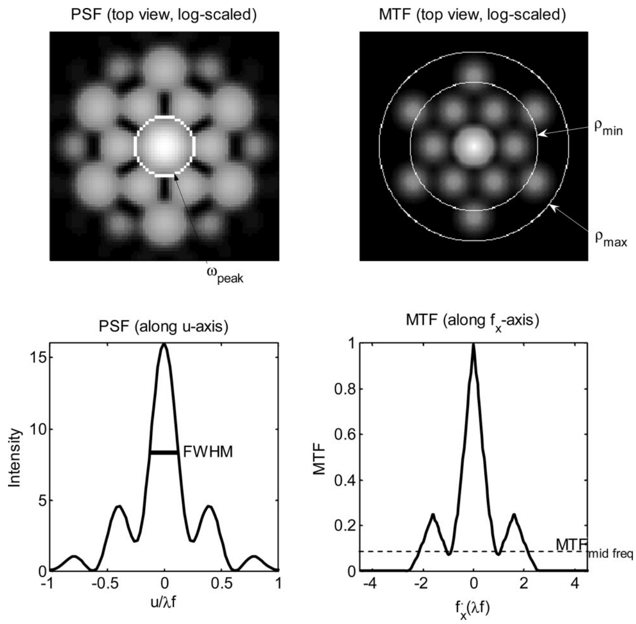

Fig. 2. Resolution metrics for a sparse array consisting of four identical, circular subapertures.

from the field of antenna design for further consideration. Referring to Fig. 2, we calculate the PISLR for a sparse aperture PSF using the following steps: First, the FWHM of the sparse aperture array's PSF is found. This determines the effective diameter, D_{eff}, from Eq. (4). Next, we construct a fictional Airy intensity pattern whose central lobe diameter, ω_{peak} is given by

$$\omega_{peak} = \frac{2.44\lambda f}{D_{eff}}. \qquad (5)$$

The PISLR is then the ratio of the sparse aperture PSF energy within the circle of diameter ω_{peak} to the energy outside this circle, expressed in decibels as

$$\mathrm{PISLR} = 10\log\left[\frac{\int_0^{2\pi}\int_0^{\omega_{peak}} \mathrm{PSF}_{array}(\rho,\ \phi)\rho d\rho d\phi}{\int_0^{2\pi}\int_{\omega_{peak}}^{\infty} \mathrm{PSF}_{array}(\rho,\ \phi)\rho d\rho d\phi}\right], \qquad (6)$$

where ρ and ϕ are cylindrical coordinates based on the u, v image plane variables.

B. Frequency Plane (Modular Transfer Function) Metrics

Useful resolution measures can also be made in the spatial frequency domain. For an incoherent imaging system, the spatial frequency content of the image is equal to the product of the spatial frequency content of the ideal geometric image and the optical transfer function (OTF), where the OTF is the normalized Fourier transform of the intensity PSF given as

$$\mathrm{OTF} \equiv \mathcal{H}(f_x, f_y) \equiv \frac{\mathcal{F}\{\mathrm{PSF}_{array}(u, v)\}}{\iint \mathrm{PSF}_{array}(u, v)\mathrm{d}u\mathrm{d}v}, \quad (7)$$

and where $f_x = x/\lambda f$ and $f_y = y/\lambda f$ are spatial frequencies [11]. The modulus of the OTF, known as the MTF describes the transfer of object contrast to an image as a function of spatial frequency. The MTF proves to be an especially useful metric in evaluating sparse aperture imaging systems. The OTF of a sparse aperture array is found by using Eq. (3) in Eq. (7). If the array consists of N identical, circular, in-phase subapertures then the OTF and MTF are equivalent and can be shown to be

$$\mathrm{MTF}_{array}(f_x, f_y) = \mathrm{MTF}_{sub}(f_x, f_y) * \left[\delta(f_x, f_y) + \frac{1}{N}\sum_{k=1}^{N(N-1)/2} \times \delta\left(f_x \pm \frac{\Delta x_k}{\lambda f}, f_y \pm \frac{\Delta y_k}{\lambda f}\right)\right], \quad (8)$$

where $\mathrm{MTF}_{sub}(f_x, f_y)$ is the MTF of a single circular aperture given by

$$\mathrm{MTF}_{sub}(\rho) = \begin{cases} \frac{2}{\pi}\left[\arccos\left(\frac{\lambda f}{D}\rho\right) - \left(\frac{\lambda f}{D}\rho\right)\sqrt{1-\left(\frac{\lambda f}{D}\rho\right)^2}\right] & \text{for } \rho \leq \frac{D}{\lambda f} \\ 0 & \text{for } \rho > \frac{D}{\lambda f}' \end{cases} \quad (9)$$

where $\rho = \sqrt{f_x^2 + f_y^2}$ is the radial spatial frequency, and $*$ denotes convolution [11]. Any aberrations within a subaperture will necessarily reduce $\mathrm{MTF}_{sub}(f_x, f_y)$, while phase errors between the subapertures, such as piston or tilt, will reduce the overall $\mathrm{MTF}_{array}(f_x, f_y)$. An ideal MTF has a constant value over an infinite spatial frequency bandwidth, corresponding to an ideal delta function PSF. However, any practical imaging system will have a finite pupil that will limit the overall MTF spatial frequency bandwidth and reduce image contrast at all spatial frequencies relative to the background.

Referring to Fig. 2, the array's MTF has a maximum spatial frequency $\rho_{\max}$ proportional to the maximum baseline dimension D_{span}. However, this maximum spatial frequency is attainable for only certain azimuth angles. We define $\rho_{\max}$ as the diameter of the smallest circle that circumscribes the entire MTF pattern and $\rho_{\min}$ as the diameter of the largest circle inscribed within the contiguous portion of the MTF. An effective diameter, D_{eff}, can then be defined based on the MTF's spatial frequency cutoff. Some have chosen a single, characteristic MTF cutoff frequency based on $\rho_{\min}$, $\rho_{\max}$, or a mean of $\rho_{\min}$ and $\rho_{\max}$ [5,7]. We select the most conservative measure, $\rho_{\min}$, as the cutoff frequency. The effective diameter can then be defined by

$$D_{eff(MTF)} = \frac{\rho_{\min}}{\rho_o} = \rho_{\min}\lambda f, \quad (10)$$

where $\rho_o = (\lambda f)^{-1}$ is the cutoff frequency for a circular, unit diameter aperture. In all cases, Eq. (10) will determine a smaller D_{eff} than Eq. (4). Therefore, to provide the most conservative results in all following discussions, Eq. (10) will be used in conjunction with Eq. (1) to determine the array fill factor α.

Spatial resolution is not the only figure of merit for an imaging system. Detection noise also has a major impact on image quality. Any practical sparse aperture imaging system contends with degraded signal to noise ratio (SNR) compared to a filled aperture for two primary reasons: first is the obvious reduction in the photon collecting area, and second is midfrequency MTF attenuation [12]. The reduction in the photon collecting area reduces the SNR of the entire image spectrum including the background. MTF attenuation, however, causes further SNR reduction within the midfrequency spectrum due to loss of image contrast, as compared to a single filled aperture. Therefore, we strive to maximize the MTF spatial frequency bandwidth while simultaneously requiring that the MTF level across the full spectrum be sufficient to achieve an acceptable imaging system SNR.

A sparse aperture array consisting of unit diameter subapertures has an MTF with a unit value at zero frequency and a volume proportional to the total aperture area. We can reduce the array's fill factor in order to increase bandwidth, but we do so at the cost of reducing MTF values for spatial frequencies greater than zero. We therefore define $\mathrm{MTF}_{midfreq}$, as the mean MTF level over spatial frequencies from unit spatial frequency to $\rho_{\min}$ as shown graphically in Fig. 2 and as calculated analytically by

$$\mathrm{MTF}_{midfreq} = \frac{1}{2\pi(\rho_{\min}^2 - 1)}\int_0^{2\pi}\int_1^{\rho_{\min}} \mathrm{MTF}(\rho, \phi)\rho\mathrm{d}\rho\mathrm{d}\phi. \quad (11)$$

We, along with other investigators, have observed that the $\mathrm{MTF}_{midfreq}$ of a well designed sparse aperture array is approximately directly proportional to the fill factor α [12]. Decreasing an array's fill factor reduces $\mathrm{MTF}_{midfreq}$, which in turn corresponds to a worse SNR.

3. Designing Optimal Sparse Aperture Arrays

The desire to image extended targets of unknown spatial frequency content would suggest that a sparse aperture array be designed to possess an MTF with maximum spatial frequency cutoff and with sufficient contrast. The MTF of a sparse aperture array is the modulus of the normalized autocorrelation of the array. Because autocorrelation is not an invertible operation, an array that generates the desired MTF cannot be calculated analytically and numerical optimization algorithms are computationally prohibitive for arrays with more than a few subapertures [13]. Golay used a random guessing algorithm and

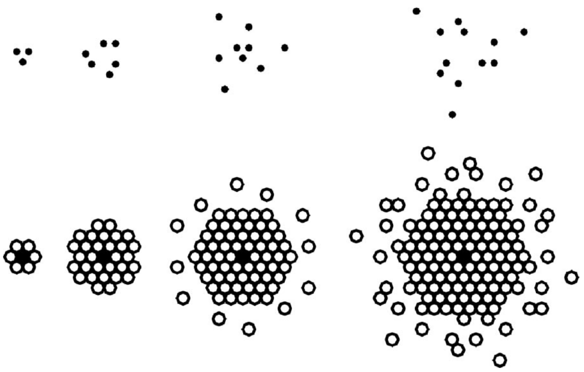

Fig. 3. Threefold symmetric Golay arrays with compact nonredundant autocorrelations. Top row: Point array configurations. Bottom row: Associated autocorrelations.

restricted his solution sets to various grid patterns in his search for point arrays having compact nonredundant autocorrelations [4,13]. Arrays with compact nonredundant autocorrelations provide the most efficient means of maximizing spatial frequency bandwidth with the fewest number of subapertures. We examined practical sparse aperture arrays constructed by centering identical circular subapertures on each of the points in Golay's threefold symmetric arrays. These arrays have particularly compact autocorrelations and low fill factors, which helps in reducing overall system complexity. The four most promising arrays along with their autocorrelations are shown in Fig. 3. In addition, the (x_n, y_n) center coordinates are provided in Table 1 for a unity expansion factor.

Table 1. Threefold Symmetric Golay Array Subaperature Center Coordinates (s = 1)

Golay-3	$\left(-\frac{1}{2}, -\frac{\sqrt{3}}{6}\right)$	$\left(\frac{1}{2}, -\frac{\sqrt{3}}{6}\right)$	$\left(0, \frac{\sqrt{3}}{3}\right)$
Golay-6	$\left(0, -\frac{2\sqrt{3}}{3}\right)$	$\left(1, -\frac{2\sqrt{3}}{3}\right)$	$\left(1, \frac{\sqrt{3}}{3}\right)$
	$\left(\frac{1}{2}, -\frac{5\sqrt{3}}{6}\right)$	$\left(-1, -\frac{\sqrt{3}}{3}\right)$	$\left(-\frac{3}{2}, \frac{-\sqrt{3}}{6}\right)$
Golay-9	$\left(-\frac{1}{2}, -\frac{\sqrt{3}}{6}\right)$	$\left(\frac{1}{2}, -\frac{\sqrt{3}}{6}\right)$	$\left(0, \frac{\sqrt{3}}{3}\right)$
	$\left(\frac{7}{2}, -\frac{\sqrt{3}}{6}\right)$	$\left(\frac{3}{2}, \frac{5\sqrt{3}}{6}\right)$	$\left(-\frac{3}{2}, \frac{11\sqrt{3}}{6}\right)$
	$\left(-2, \frac{\sqrt{3}}{3}\right)$	$\left(-2, -\frac{5\sqrt{3}}{3}\right)$	$\left(\frac{1}{2}, -\frac{7\sqrt{3}}{6}\right)$
Golay-12	$(0, -\sqrt{3})$	$(-2, -\sqrt{3})$	$\left(-\frac{1}{2}, -\frac{3\sqrt{3}}{2}\right)$
	$(-4, -2\sqrt{3})$	$(5, -\sqrt{3})$	$\left(\frac{5}{2}, -\frac{\sqrt{3}}{2}\right)$
	$\left(\frac{5}{2}, \frac{\sqrt{3}}{2}\right)$	$\left(\frac{3}{2}, \frac{\sqrt{3}}{2}\right)$	$\left(-\frac{1}{2}, \frac{3\sqrt{3}}{2}\right)$
	$\left(-\frac{3}{2}, \frac{\sqrt{3}}{2}\right)$	$(-2, \sqrt{3})$	$(-1, 3\sqrt{3})$

A. Optimizing the Expansion Factor

The effect of placing circular pupils on a Golay point array is directly influenced by the expansion factor. The MTF of a Golay array with an expansion factor of unity is tightly filled about the origin with few frequency plane voids and also exhibits a favorable, nearly uniform MTF level over all midband spatial frequencies. Increasing the expansion factor of an array has a predictable effect on its MTF. If in Eq. (8), we initially assume the vector separation components describe an array where the closest pupil subapertures are tangent ($s = 1$), then Δx_k, Δy_k, are simply scaled by the expansion factor, becoming simply $s\Delta x_k$ and $s\Delta y_k$ for nonunity expansion factors.

Table 2 presents the properties of a Golay-9 array. Each row lists the PSF and MTF metrics for an increasing expansion factor. As expected, there is a linear increase in D_{eff} based on the FWHM of the PSF and a linear increase in the cutoff frequencies, $\rho_{\min}$ and $\rho_{\max}$ of the MTF. Generally then, the expansion factor can be increased in order to maximize bandwidth until voids appear in the MTF. For example, the Golay-9 array has MTF voids that appear when the expansion factor is increased beyond 1.6. For this study, we chose expansion factors slightly less than that required to avoid zero MTF levels. Specifically, we set the expansion factor so that the minimum MTF level was approximately 3% of the peak. As previously mentioned, in a practical imaging system, the array would be required to maintain a minimum MTF level based on SNR considerations, instead of simply avoiding zero MTF levels.

B. Comparison of Subaperture Arrangements

The most promising arrays due to the compactness of their autocorrelations/MTFs are the threefold symmetric Golay-3, -6, -9, and -12 arrays. Each of these arrays has been optimized for an expansion factor. Top views of each array's PSF and MTF are shown in the grayscale plots of Figs. 4 to 7, along with a central horizontal slice of each function appearing below. The salient PSF and MTF measures for a single subaperture and each of these Golay arrays are also provided in Table 3. Recall that the merit of a sparse aperture imaging system with respect to diffraction-limited performance is the fill factor, while the merit of a sparse aperture imaging system with respect to SNR performance is quantified by the $\mathrm{MTF}_{midfreq}$. The Golay-9 and Golay-12 arrays will clearly have the best diffraction performance with low, nearly identical fill factors. However, the $\mathrm{MTF}_{midfreq}$ performance of the Golay-9 array is superior to the Golay-12, meaning that images captured by the Golay-9 array should have better average contrast. Therefore, the Golay-9 with an expansion factor of 1.4 is considered by us to be the best array because it synthesizes a large D_{eff} for a relatively modest 27.9% fill factor, while also maintaining adequate midfrequency contrast. The geometry of this array is shown in Fig. 8.

Table 2. Golay-9 Array Metrics as a Function of Expansion Factor *s*

Array	Expansion Factor (s)	$D_{\text{circumscribed}}$	FWHM_{PSF}	PISLR [dB]	$\rho_{\min}(\lambda f)$	$\rho_{\max}(\lambda f)$	$\text{MTF}_{midfreq}$	Fill Factor (α) (%)
Golay-9	1.0	8.02	$\delta_0/6.98$	−6.14	4.36	7.08	0.089	47.2
Golay-9	1.1	8.73	$\delta_0/7.58$	−7.09	4.71	7.68	0.076	40.6
Golay-9	1.2	9.43	$\delta_0/8.16$	−7.94	5.02	8.29	0.067	35.7
Golay-9	1.3	10.1	$\delta_0/8.77$	−8.70	5.32	8.90	0.059	31.9
Golay-9	1.4	10.8	$\delta_0/9.38$	−9.39	5.68	9.50	0.052	27.9
Golay-9	1.5	11.5	$\delta_0/9.98$	−10.0	5.92	10.1	0.046	25.7
Golay-9	1.6	12.2	$\delta_0/10.6$	−10.6	6.23	10.8	0.041	23.2
Golay-9	1.7	12.9	$\delta_0/12.7$	−11.4	2.12	11.4	Voids	—
Golay-9	1.8	13.6	$\delta_0/13.4$	−11.9	1.66	12.2	Voids	—
Golay-9	1.9	14.3	$\delta_0/14.1$	−12.4	1.20	12.7	Voids	—
Golay-9	2.0	15.0	$\delta_0/14.8$	−12.8	1.18	13.2	Voids	—

4. Aberration Errors in a Sparse Aperture Imaging System

Piston and/or tilt phase errors added to one or more of the subapertures generally degrades resolution. To examine the effects such phase errors have on the array's incoherent PSF, we numerically found the modulus squared of the Fourier transform of Eq. (2), after first applying the desired phase structure to each of the subapertures. The array MTF was then examined by numerical evaluation of Eq. (7) and taking the modulus of the result.

Figure 9 shows the PSF and MTF of the optimized Golay-9 array when a half wave of piston has been added to the inner, lower left subaperture of the array shown in Fig. 8. The effect on the PSF is quite noticeable, as energy is displaced from the central peak to the sidelobes [9]. The MTF also suffers from the added piston. Notice in Fig. 9 that the MTF level in areas between the point autocorrelation peaks is reduced from that seen in Fig. 6. Fortunately, a half wave of piston is the worst case scenario for a single subaperture.

Figure 10 shows the PSF and MTF of the Golay-9 array when the same subaperture has been tilted along the horizontal axis by a full wave. The full wave of tilt on a single subaperture causes the energy from that subaperture to be deflected away from the optic axis, placing energy into the sidelobes of the PSF and thereby degrading resolution. The MTF also suffers from tilt as seen by the frequency voids that appear. As expected, if a sparse aperture system is to provide resolution gain, the subapertures must be phased to within interferometric tolerances.

5. Imaging a Resolution Target

A transmissive ISO12233 resolution chart was imaged onto a focal plane array through an optimized Golay-9 sparse aperture array [14]. The image of this chart provided a means to directly measure the MTF of the array. The optical arrangement of the experi-

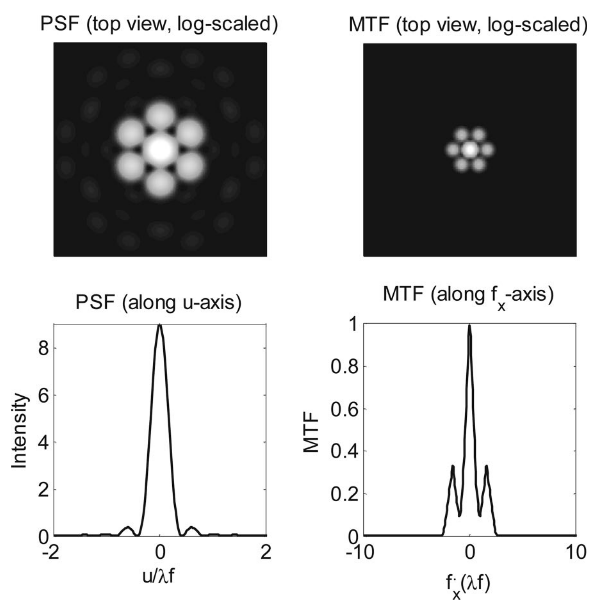

Fig. 4. PSF and MTF for a Golay-3 array with an optimum expansion factor of 1.6.

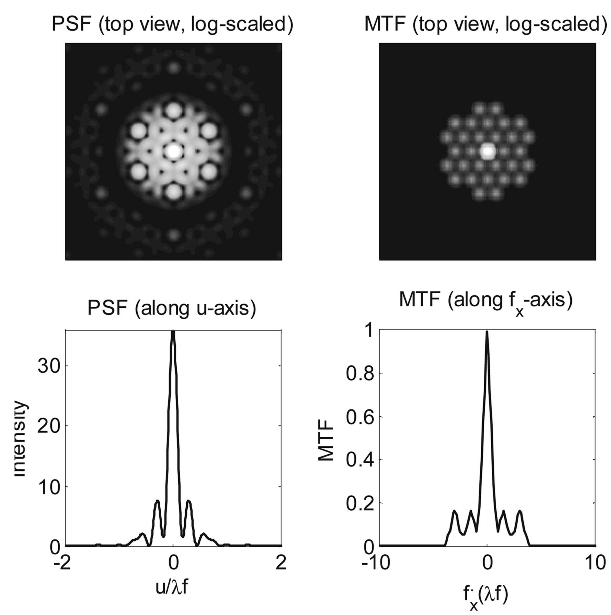

Fig. 5. PSF and MTF for a Golay-6 array with an optimum expansion factor of 1.5.

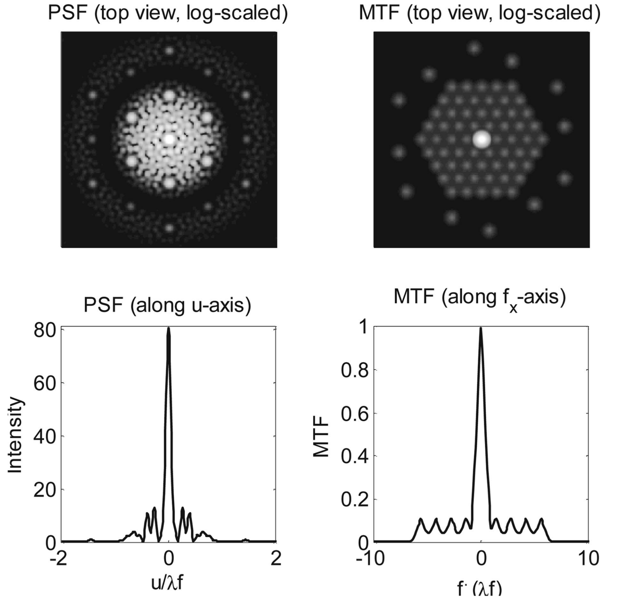

Fig. 6. PSF and MTF for a Golay-9 array with an optimum expansion factor of 1.4.

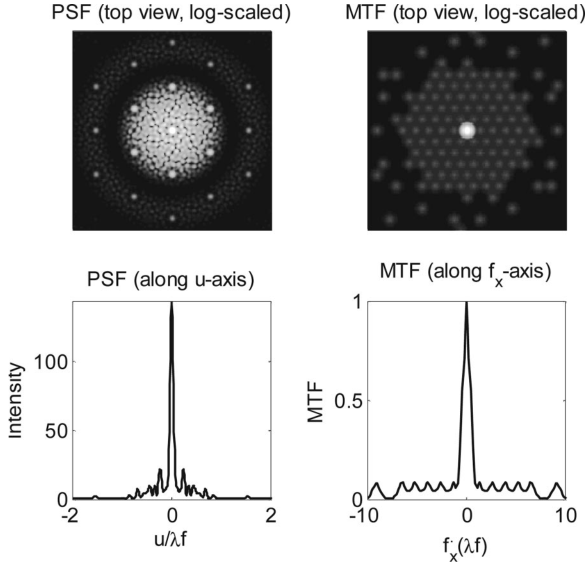

Fig. 7. PSF and MTF for a Golay-12 array with an optimum expansion factor of 1.3.

ment is shown in Fig. 11. The incoherently illuminated target was placed one focal length in front of lens f_1. In this way, the $4f$ system then effectively places the resolution target at an infinite distance from the f_2 lens/pupil plane mask combination being evaluated. The magnification of this imaging system is the ratio of lens focal lengths, f_2/f_1. High optical quality achromatic doublets were used in order to avoid aberrations that would adversely affect performance, and a monochrome CCD camera (1600 × 1200 pixels at a 4.4 μm pixel pitch) with a nominally linear 8 bit response was used to capture the images.

The pupil of this simple imaging system is coincident with lens f_2. Therefore, the Golay-9 ($s = 1.4$) pupil mask was placed as close as possible (approximately 7 mm) from the front surface of this lens. An image of the slant bars in the ISO12233 target was then used to calculate the MTF using a commonly accepted algorithm [15]. This algorithm takes the image of the slant bar edge, finds a line of best fit via least squares error, and constructs an averaged edge profile. The derivative of the edge profile is then calculated to obtain the line spread function. Next, a discrete Fourier transform is applied to the line spread function, and the result is scaled by the pixel sampling size giving the MTF normal to the slant edge. The MTF was calculated by this method using a software analysis tool available from the International Imaging Industry Association [16].

Experimental results are shown in Fig. 12 where the horizontal and vertical MTFs were calculated from the two slant bar features in the captured image and are plotted along with the theoretical MTFs for the Golay-9 array. The measured MTFs agree quite well with the theoretical MTFs at all spatial frequencies. In addition, a portion of the raw image captured

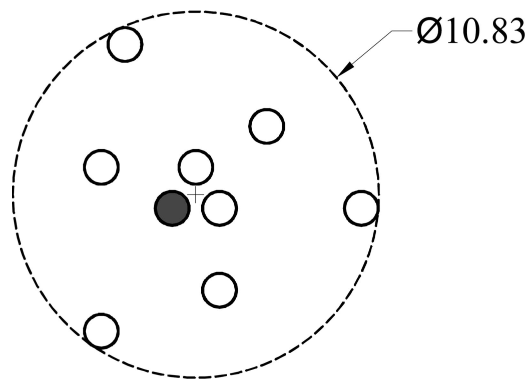

Fig. 8. Golay-9 array geometry for an optimum expansion factor of 1.4.

Table 3. Quality Measures of Optimized *N* Element Golay Arrays

Array	Expansion Factor (s)	$D_{\text{circumscribed}}$	FWHM_{PSF}	PISLR [dB]	$\rho_{\min}(\lambda f)$	$\rho_{\max}(\lambda f)$	$\text{MTF}_{midfreq}$	Fill Factor (α)
Single	NA	1.00	δ_0	7.13	1.00	1.00	NA	1.00
Golay-3	1.6	2.85	$\delta_0/2.92$	−2.92	1.99	2.60	0.136	75.8%
Golay-6	1.5	5.58	$\delta_0/5.83$	−7.52	3.98	4.96	0.067	37.9%
Golay-9	1.4	10.8	$\delta_0/9.38$	−9.39	5.68	9.50	0.052	27.9%
Golay-12	1.3	14.8	$\delta_0/12.7$	−10.6	6.59	12.9	0.045	27.6%

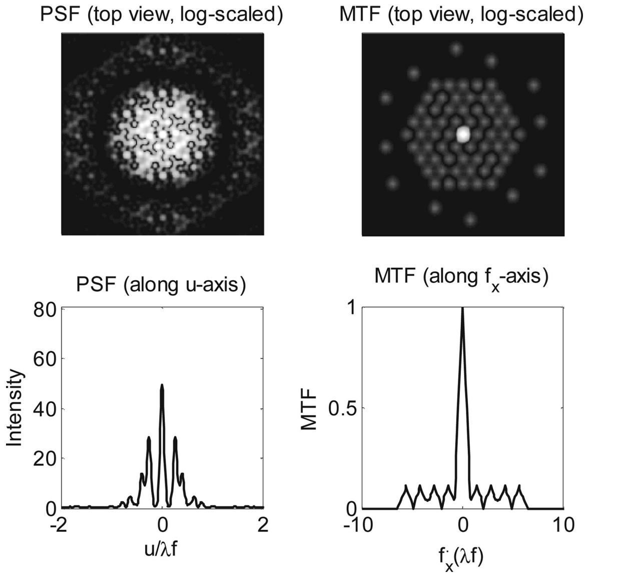

Fig. 9. PSF and MTF of the optimized Golay-9 array with $\lambda/2$ piston added to one subaperture.

through the Golay-9 array is shown on the left hand side of Fig. 13. Though the image has increased resolution compared to that of a single subaperture, it is not subjectively pleasing due to its low contrast. Reduced contrast is inherent to sparse arrays with low fill factors: a reduction in midband MTF directly corresponds to a reduction in image contrast. We therefore expect that a practical sparse aperture imaging system would employ a postdetection restoration filter to improve image contrast [6]. In theory, the ideal geometric optics image can be restored by a deconvolution of the image detected at the focal plane with the known PSF of the imaging system. For practical imaging systems, improved restoration filters such as

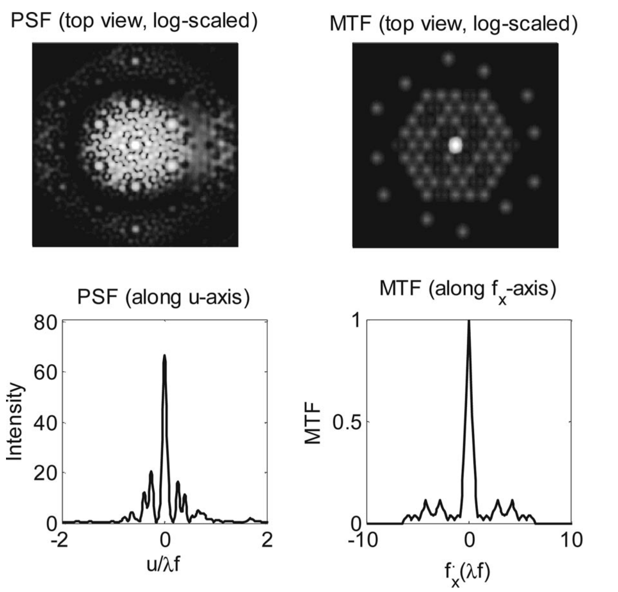

Fig. 10. PSF and MTF of the optimized Golay-9 array with λ tilt added to one subaperture.

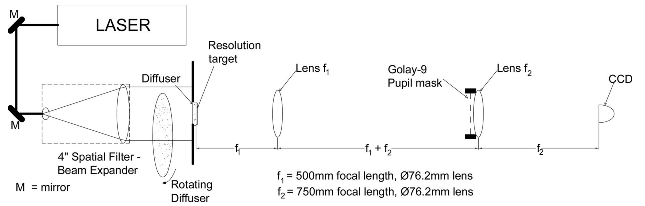

Fig. 11. Imaging of an incoherently illuminated resolution target through a Golay aperture array.

the Wiener–Helstrom filter are used, which account for the presence of noise in the detected image [17]. A Wiener restoration filter, $W(f_x, f_y)$, which deconvolves the detected image with the known imaging system PSF in the presence of white noise is given by

$$W(f_x, f_y) = \frac{\mathcal{H}^*(f_x, f_y)}{|\mathcal{H}(f_x, f_y)|^2 + K}, \tag{12}$$

where $\mathcal{H}(f_x, f_y)$ is the OTF and K is the ratio of the noise power to the average image signal power. Note that the Wiener filter can improve image contrast but cannot recover image spatial frequency content below the noise floor. The results of applying a Wiener filter to our raw image can be seen on the right hand side of Fig. 13, where K was selected to provide a subjectively pleasing image.

6. Synthesis of Focal Plane Images

In Section 5 we have experimentally verified that high resolution images can be synthesized by combining the fields at each of the subapertures onto a single focal plane detector array. Such an imaging system is shown schematically in Fig. 14(a), in which the pupil plane field is simultaneously sampled by multiple subapertures. The superposition of the images formed by each of the subaperture *fields* is centered on the optic axis of the focal plane by virtue of the large imaging lens. The image intensity detected by the focal plane array is then simply the squared modulus of this superposition field. Proper synthesis of the subaperture pupil plane fields requires phasing the subaperture fields to within interferometric tolerances, which the large imaging lens does directly. Unfortunately, the single large imaging lens defeats one of the primary reasons for pursuing sparse aperture imaging, namely, eliminating the cost, weight, and area of a large monolithic optic. Others have constructed sparse aperture imaging systems using multiple, smaller optics to coherently combine subaperture fields onto a single detector, such as the Air Force Research Laboratory's Multipurpose Multiple Telescope Testbed (MMTT), and MIT's Adaptive Reconnaissance Golay-3 Optical Satellite (ARGOS) [9]. Both systems use sensing techniques that provide feedback to actively control an optical beam combiner. An alternative sparse aperture imaging system that combines intensity images captured by multiple, spatially separated cameras is shown schematically in Fig. 14(b). In this system the pupil field is sampled by multiple independent cameras, which

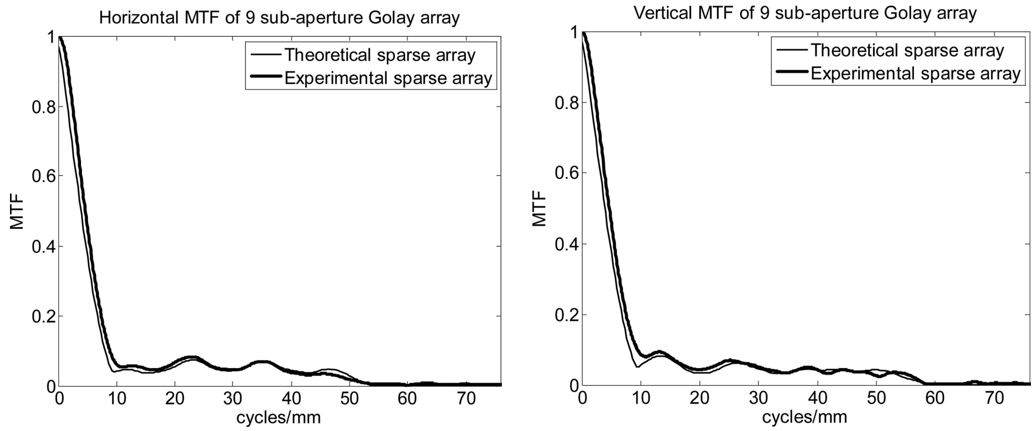

Fig. 12. Measured and theoretical MTF cross-sections for the optimized Golay-9 array ($s = 1.4$).

are shown composed of simple lenses and CCD arrays.

A. Process Description

A CCD focal plane array senses time averaged intensity, not complex field. With only modulus information available in the focal plane, we lack complete knowledge of the pupil plane field. The phase can be measured with more sophisticated coherent imaging methods, such as holographic imaging or heterodyne detection [18]. In the interest of experimental simplicity, however, we chose to employ one of the well known phase retrieval algorithms to construct an estimate of the pupil field for each subaperture based on its measured focal plane intensity [19]. In conjunction with the phase retrieval algorithm, the discrete cameras are then essentially wavefront sensors that measure the pupil plane field at each subaperture location.

Referring to Fig. 14(b), intensity images of a coherently illuminated object are simultaneously captured on multiple, identical focal plane CCD detectors. The modulus of the detected focal plane fields are found by taking the square root of each intensity image. This focal plane modulus and the known aperture shape are the constraints that are then used in an iterative Fourier-transform phase retrieval algorithm that yields an estimate of the complex field at each camera's pupil [20]. During postprocessing, the retrieved subaperture fields are then placed in a single matrix at a location corresponding to the camera's physical position in the sparse aperture array. A higher resolution image is synthesized digitally by applying a virtual lens to the spatially separated fields and propagating the composite pupil plane field to a virtual focal plane detector and forming the image plane field via discrete Fourier transform. The synthesized image is the modulus squared of the result.

B. Experimental Synthesis of a Point Object Image

We used the system described in Fig. 15 to image a distant point object that was approximated by a Gaussian plane wave created by spatially filtering and collimating the output of a Nd:YAG laser. To simplify the experiment an optimized ($s = 1.6$) Golay-3 mask was placed in the pupil plane, a single subaperture was uncovered, and an image was cap-

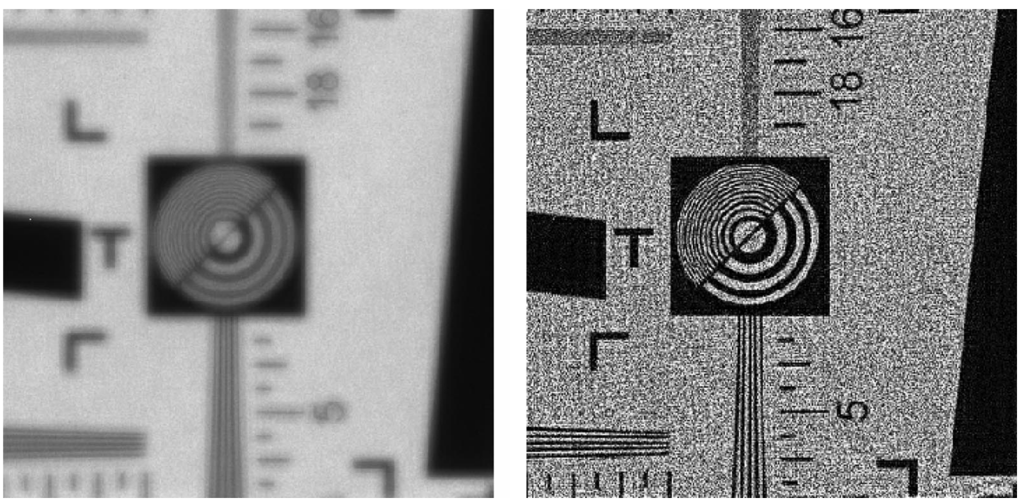

Fig. 13. A raw Golay-9 image (left) and its Wiener restored image (right).

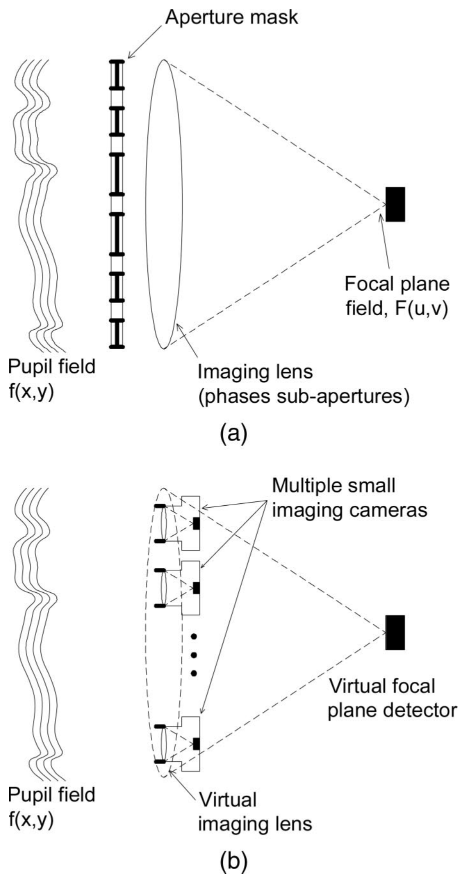

Fig. 14. (a) Image synthesis using a single real imaging lens. (b) Postdetection image synthesis using a virtual imaging lens.

tured by the CCD. An image corresponding to each subaperture was then captured sequentially. The pupil plane field (amplitude and phase) was reconstructed for each subaperture using the iterative Fourier-transform phase retrieval algorithm. Figure 16 is an example showing the captured focal plane images and the retrieved pupil plane phase and intensity resulting from the phase retrieval algorithm for the single subaperture labeled "B". Because we imaged a distant point source, the retrieved pupil plane fields exhibit flat phase and intensity. However, because the phase retrieval algorithm is employed separately to each subaperture intensity image, all interpupil phase relationships are lost re-

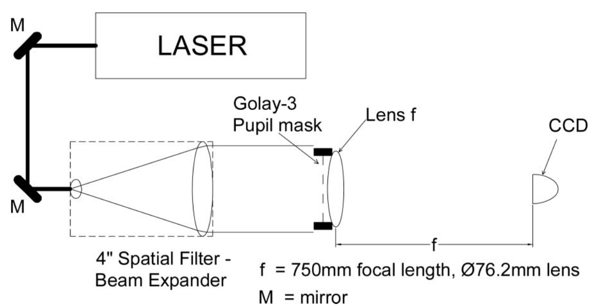

Fig. 15. Imaging of an infinite point object with a fixed Golay aperture array.

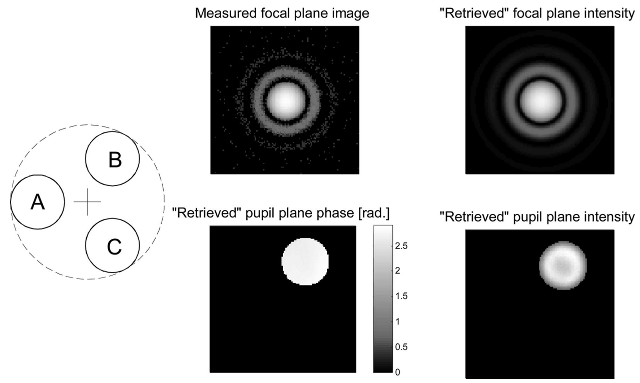

Fig. 16. Pupil plane phase and intensity retrieval for subaperture B of the Golay-3 array shown at left.

sulting in piston errors and potentially poor imaging system performance. To correct this, we subtracted the mean phase measured across each pupil in order to null the interpupil piston. Next, the correctly phased subaperture pupil fields were combined into a single matrix. The array of subaperture fields was propagated to the focal plane via discrete Fourier transform and squared to obtain the synthetic focal plane image of the point object shown in Fig. 17.

C. Potential Weaknesses of Image Synthesis Using Phase Retrieval

We observed that our implementation of the phase retrieval algorithm does not converge on a good pupil field estimate in the presence of appreciable background noise. The phase retrieval algorithm reconstructs a seemingly random, fine structure in the pupil plane phase when even a small uniform bias is added to the ideal Airy intensity in the focal plane. We suspect that this fine structure is required in the pupil in order to diffract some of the energy away from the small central Airy spot toward coverage of the entire focal plane.

Successful aperture synthesis requires coherently combining multiple subaperture pupil fields. To coherently combine these fields during postdetection processing, the phase relationships between subaperture pupils must be known. Therefore, the pupil

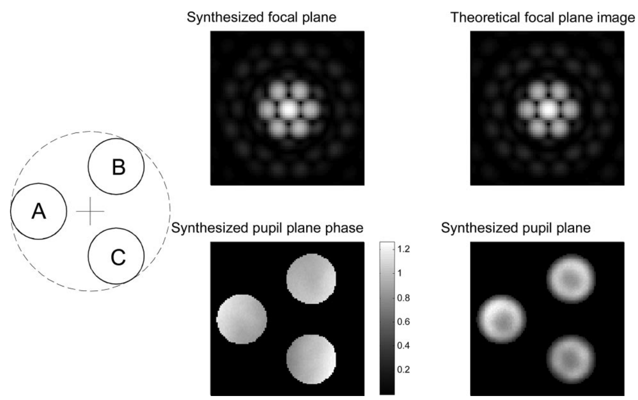

Fig. 17. Postdetection synthesis of Golay-3 intensity images.

plane field must be spatially coherent over the entire sparse aperture and temporally coherent over the exposure time of the CCD focal plane array. The point source object of our experiment yields a spatially coherent pupil field, but the radiation from an extended object will generally not possess spatial coherence over the entire pupil. Therefore, in order to maintain phase relationships between separated subapertures, the object must be coherently illuminated. Coherent illumination presents some potential concerns. First, the phase retrieval algorithm must reconstruct a complex-valued pupil field from the focal plane image intensity, a task the algorithm finds difficult [21]. Second, since the pupil phase will likely contain fine structure, a more sophisticated piston and tilt nulling routine will need to be designed. Third, coherent illumination introduces speckle into the focal plane image. Speckle's high contrast is generally quite bothersome in an image, though it can be reduced by averaging over multiple realizations, thereby spoiling the spatial coherence of the composite image. However, this requires increased total exposure time and more elaborate postdetection image synthesis processing in order to construct a higher resolution image.

7. Summary and Conclusions

We have defined resolution metrics based on the PSF and MTF to evaluate sparse arrays of N identical, diffraction-limited subapertures. The effects of detection noise, image restoration filtering, and piston and/or tilt aberrations were investigated with respect to sparse aperture imaging. We selected compact nonredundant autocorrelation Golay arrays for which we adjusted both the number of subapertures and their relative spacings to arrive at an optimized threefold symmetric Golay-9 array. We then synthesized an image from multiple subaperture pupil fields by masking a large lens with this Golay-9 array. We imaged a slant edge resolution target to verify the resolution gain of the Golay-9 array as quantified by its MTF. We also successfully applied a restoration filter to our image in order to recover lost contrast. We then described a synthesis method that uses a phase retrieval algorithm and presented experimental results for the imaging of a distant point object. Weaknesses of applying this method were discussed.

Sparse aperture imaging has been shown to enhance resolution over a single monolithic aperture of equal total area. However, we have observed that sparse aperture arrays have reduced SNR and present the formidable technical challenge of accurately phasing the various subapertures. The possibility of postdetection synthesis of images through the use of phase retrieval is possible and was explored. However, in our experiments, phase retrieval image synthesis was successful only for rudimentary, distant point source imaging.

This effort was supported in part by the U.S. Air Force and General Dynamics, of Dayton, Ohio through contract F33601-02-F-A581, and by the Ladar and Optical Communications Institute (LOCI) at the University of Dayton. The views expressed in this paper are those of the authors and do not reflect on the official policy of the Air Force, Department of Defense, or the U.S. government.

References

1. J. D. Monnier, "Optical interferometry in astronomy," Rep. Prog. Phy. **66,** 789–857 (2003).
2. J. W. Goodman, *Statistical Optics,* 1st ed. (Wiley-Interscience, 1985).
3. A. A. Michelson, *Studies in Optics* (University of Chicago Press, 1927).
4. M. J. E. Golay, "Point arrays having compact nonredundant autocorrelations," J. Opt. Soc. America **61,** 272–273 (1971).
5. R. D. Fiete, T. Tantalo, J. R. Calus, and J. A. Mooney, "Image quality of sparse-aperture designs for remote sensing," in Opt. Eng. **41,** 1957–1969 (2002).
6. L. M. Mugnier, G. Rousset, and F. Cassaing, "Aperture configuration optimality criterion for phased arrays of optical telescopes," J. Opt. Soc. Am. A **13,** 2367–2374 (1996).
7. J. E. Harvey and R. A. Rockwell, "Performance characteristics of phased array and thinned aperture telescopes," Opt. Eng. **27,** 762–768 (1988).
8. J. L. Flores, G. Paez, and M. Strojnik, "Design of a diluted aperture by use of the practical cutoff frequency," Appl. Opt. **38,** 6010–6018 (1999).
9. S.-J. Chung, D. W. Miller, and O. L. deWeck, "Design and implementation of sparse aperture imaging systems," in *Highly Innovative Space Telescope Concepts,* H. A. MacEwen, ed., Proc. SPIE **4849,** 181–192 (2002).
10. S. M. Watson, J. P. Mills, and S. K. Rogers, "Two-point resolution criterion for multiaperture optical telescopes," J. Opt. Soc. Am. A **5,** 893–903 (1988).
11. J. W. Goodman, *Introduction to Fourier Optics,* 2nd ed. (McGraw-Hill, 1996).
12. J. R. Fienup, "MTF and integration time versus fill factor for sparse-aperture imaging systems," in *Imaging Technology and Telescopes,* J. W. Bilbro, J. B. Breckinridge, R. A. Carreras, S. R. Czyzak, M. J. Eckert, R. D. Fiete, and P. S. Idell, eds., Proc. SPIE **4091,** 43–47 (2000).
13. E. Keto, "The shapes of cross-correlation interferometers," Astrophys. J. **475,** 843–852 (1997).
14. ISO 12233, "Photography—electronic still-picture cameras—resolution measurements" (International Organization for Standardization, 2000).
15. B. Tatian, "Method for obtaining the transfer function from the edge response function," J. Opt. Soc. Am. **55,** 1014–1019 (1965).
16. P. Burns, *Spatial Frequency Response code written for Matlab, sfrmat2: version 2.1* (International Imaging Industry Association, 2003).
17. C. W. Helstrom, "Image restoration by the method of least squares," J. Opt. Soc. Am. **57,** 297–303 (1967).
18. J. W. Goodman, D. W. Jackson, M. Lehmann, and J. Knotts, "Experiments in long-distance holographic imagery," Appl. Opt. **8,** 1581–1586 (1969).
19. R. J. Fienup, "Phase retrieval algorithms: a comparison," Appl. Opt. **21,** 2758–2769 (1982).
20. J. N. Cederquist, J. R. Fienup, C. C. Wackerman, S. R. Robinson, and D. Kryskowski, "Wave-front phase estimation from Fourier intensity measurements," J. Opt. Soc. Am. A **6,** 1020–1026 (1989).
21. J. R. Fienup, "Reconstruction of a complex-valued object from the modulus of its Fourier transform using a support constraint," J. Opt. Soc. Am. A **4,** 118–123 (1987).
22. N. J. Miller, B. D. Duncan, and M. P. Dierking, "Resolution enhanced sparse aperture imaging," in *Proceedings of IEEE Aerospace Conference* (IEEE, 2006) IEEEAC paper 1406.